

Wave-equation migration velocity analysis. I. Theory

P. Sava* and B. Biondi

Department of Geophysics, Stanford University, Mitchell Building, Stanford, CA 94305-2215, USA

Received January 2004, revision accepted July 2004

ABSTRACT

We present a migration velocity analysis (MVA) method based on wavefield extrapolation. Similarly to conventional MVA, our method aims at iteratively improving the quality of the migrated image, as measured by the flatness of angle-domain common-image gathers (ADCIGs) over the aperture-angle axis. However, instead of inverting the depth errors measured in ADCIGs using ray-based tomography, we invert ‘image perturbations’ using a linearized wave-equation operator. This operator relates perturbations of the migrated image to perturbations of the migration velocity. We use prestack Stolt residual migration to define the image perturbations that maximize the focusing and flatness of ADCIGs.

Our linearized operator relates slowness perturbations to image perturbations, based on a truncation of the Born scattering series to the first-order term. To avoid divergence of the inversion procedure when the velocity perturbations are too large for Born linearization of the wave equation, we do not invert directly the image perturbations obtained by residual migration, but a linearized version of the image perturbations. The *linearized image perturbations* are computed by a linearized prestack residual migration operator applied to the background image. We use numerical examples to illustrate how the backprojection of the linearized image perturbations, i.e. the gradient of our objective function, is well behaved, even in cases when backprojection of the original image perturbations would mislead the inversion and take it in the wrong direction.

We demonstrate with simple synthetic examples that our method converges even when the initial velocity model is far from correct. In a companion paper, we illustrate the full potential of our method for estimating velocity anomalies under complex salt bodies.

INTRODUCTION

Seismic imaging is a two-step process: velocity estimation and migration. As the velocity function becomes more complex, the two steps become increasingly interdependent. In complex depth imaging problems, velocity estimation and migration are applied iteratively in a loop. To ensure that this iterative imaging process converges to a satisfactory model, it is crucial that the migration and the velocity estimation are consistent with each other.

Kirchhoff migration often fails in areas of complex geology, such as subsalt, because the wavefield is severely distorted by lateral velocity variations leading to complex multipathing. As the shortcomings of Kirchhoff migration have become apparent (O’Brien and Etgen 1998), there has been renewed interest in wave-equation migration, and computationally efficient 3D prestack depth migration methods have been developed (Biondi and Palacharla 1996; Biondi 1997; Mosher, Foster and Hassanzadeh 1997). However, no corresponding progress has been made in the development of migration velocity analysis (MVA) methods based on the wave equation. We aim at filling this gap by presenting a method that, at least in principle, can be used in conjunction with any downward-continuation migration method. In particular, we have been applying our new

Paper presented at the EAGE/SEG Summer Research Workshop, Trieste, Italy, August/September 2003.

*E-mail: paul@sep.stanford.edu

methodology to downward continuation based on the double square root (Yilmaz 1979; Claerbout 1985; Popovici 1996) or common-azimuth (Biondi and Palacharla 1996) equations.

As in the case of migration, wave-equation MVA (WEMVA) is intrinsically more robust than ray-based MVA because it avoids the well-known instability problems that rays encounter when the velocity model is complex and has sharp boundaries. The transmission component of finite-frequency wave propagation is mostly sensitive to the smooth variations in the velocity model. Consequently, WEMVA produces smooth, stable velocity updates. In most cases, no smoothing constraints are needed to ensure stability in the inversion. In contrast, ray-based methods require strong smoothing constraints to avoid divergence. These smoothing constraints often reduce the resolution of the inversion that would otherwise be possible, given the characteristics of the data (e.g. geometry, frequency content, signal-to-noise ratio, etc.). Eliminating, or substantially reducing, the amount of smoothing increases the resolution of the final velocity model.

A well-known limitation of wave-equation tomography or MVA is represented by the linearization of the wave equation based on truncation of the Born scattering series to the first-order term. This linearization is hereafter referred to as the *Born approximation*. If the phase differences between the modelled and recorded wavefields are larger than a fraction of the wavelet, then the assumptions made under the Born approximation are violated and the velocity inversion methods diverge (Woodward 1992; Pratt 1999; Dahlen, Hung and Nolet 2000; Hung, Dahlen and Nolet 2000). Overcoming these limitations is crucial for a practical MVA tool. This goal is easier to accomplish with methods that optimize an objective function that is defined in the image space (e.g. differential semblance optimization and our WEMVA) than with methods that optimize an objective function that is defined in the data space.

Our method employs the Born approximation to linearize the relationship between the velocity model and the image. However, we ‘manipulate’ the image perturbations to ensure that they are consistent with the Born approximation, and we replace the image perturbations with their linearized counterparts. We compute image perturbations by analytically linearizing our image-enhancement operator (e.g. prestack residual migration) and applying this linearized operator to the background image. Therefore, the linearized image perturbations are approximations to the non-linear image perturbations that are caused by arbitrary changes of the velocity model. Since we linearize both operators (migration and residual migration) with respect to the amplitude of the images,

the resulting linear operators are consistent with each other. Therefore, the inverse problem converges for a wider range of velocity anomalies than the one implied by the Born approximation.

Our method is more similar to conventional MVA than other proposed wave-equation methods for estimating the background velocity model (Noble, Lindgren and Tarantola 1991; Bunks *et al.* 1995; Forgues, Scala and Pratt 1998) because it maximizes the migrated image quality instead of matching the recorded data directly. We define the quality of the migrated image by the flatness of the migrated angle-domain common-image gathers (ADCIGs) along the aperture-angle axis (Sava and Fomel 2003). In this respect, our method is related to differential semblance optimization (DSO) (Symes and Carazzone 1991; Shen 2003) and multiple migration fitting (Chavent and Jacewitz 1995). With respect to DSO, our method has the advantage that at each iteration it optimizes an objective function that rewards flatness in the ADCIGs globally (for all the angles at the same time), and not just locally as DSO does (minimizing the discrepancies between the image at each angle and the image at the adjacent angles). We suggest that this characteristic should speed up the convergence, although we have no formal proof of our assertion.

This paper describes the theoretical foundations of wave-equation MVA with simple examples illustrating the main concepts and techniques. In a companion paper (Sava and Biondi 2004), we present an application of wave-equation MVA to the challenging problem of velocity estimation under salt. Here, we begin by discussing wavefield scattering in the context of one-way wavefield extrapolation methods. Next, we introduce the objective function for optimization and finally, we address the limitations introduced by the Born approximation. Two appendices detail the wave-equation MVA process and the computation of linearized image perturbations.

RECURSIVE WAVEFIELD EXTRAPOLATION

Imaging by wavefield extrapolation (WE) is based on recursive continuation of the wavefields \mathcal{U} from a given depth level to the next by means of an extrapolation operator \mathbf{E} , i.e.

$$\mathcal{U}_{z+\Delta z} = \mathbf{E}_z [\mathcal{U}_z]. \quad (1)$$

Here and hereafter, we use the following notation conventions: $\mathbf{A}[x]$ denotes operator \mathbf{A} applied to x , and $f(x)$ denotes function f of argument x . The subscripts z and $z + \Delta z$ indicate quantities corresponding to the depth levels z and $z + \Delta z$, respectively.

The recursive equation (1) can also be explicitly written in matrix form as

$$\begin{pmatrix} 1 & 0 & 0 & \cdots & 0 & 0 \\ -\mathbf{E}_0 & 1 & 0 & \cdots & 0 & 0 \\ 0 & -\mathbf{E}_1 & 1 & \cdots & 0 & 0 \\ \vdots & \vdots & \vdots & \ddots & \vdots & \vdots \\ 0 & 0 & 0 & \cdots & -\mathbf{E}_{n-1} & 1 \end{pmatrix} \begin{pmatrix} \mathcal{U}_0 \\ \mathcal{U}_1 \\ \mathcal{U}_2 \\ \vdots \\ \mathcal{U}_n \end{pmatrix} = \begin{pmatrix} \mathcal{D}_0 \\ 0 \\ 0 \\ \vdots \\ 0 \end{pmatrix}$$

or in a more compact notation as

$$(\mathbf{1} - \mathbf{E})\mathcal{U} = \mathcal{D}, \quad (2)$$

where the vector \mathcal{D} represents data, \mathcal{U} represents the extrapolated wavefield at all depth levels, \mathbf{E} denotes the extrapolation operator and $\mathbf{1}$ is the identity operator. Here and hereafter, we make the distinction between quantities measured at a particular depth level (e.g. \mathcal{U}_z), and the corresponding vectors denoting such quantities at all depth levels (e.g. \mathcal{U}).

After wavefield extrapolation, we obtain an image by applying, at every depth level, an imaging operator (\mathbf{I}_z) to the extrapolated wavefield \mathcal{U}_z :

$$\mathcal{R}_z = \mathbf{I}_z[\mathcal{U}_z], \quad (3)$$

where \mathcal{R}_z denotes the image at some depth level. A commonly used imaging operator \mathbf{I}_z involves summation over the temporal frequencies. We can write the same relationship in compact matrix form as

$$\mathcal{R} = \mathbf{I}\mathcal{U}, \quad (4)$$

where \mathcal{R} denotes the image, and \mathbf{I} denotes the imaging operator which is applied to the extrapolated wavefield \mathcal{U} at all depth levels.

If a perturbation of the wavefield is applied at some depth level, $\Delta\mathcal{U}$ can be derived from the background wavefield by a simple application of the chain rule of derivation to (1), i.e.

$$\Delta\mathcal{U}_{z+\Delta z} = \mathbf{E}_z[\Delta\mathcal{U}_z] + \Delta\mathcal{V}_{z+\Delta z}, \quad (5)$$

where $\Delta\mathcal{V}_{z+\Delta z} = \Delta\mathbf{E}_z[\mathcal{U}_z]$ represents the scattered wavefield generated at $z + \Delta z$ by the interaction of the wavefield \mathcal{U}_z with a perturbation of the velocity model at depth z . $\Delta\mathcal{U}_{z+\Delta z}$ is the accumulated wavefield perturbation corresponding to slowness perturbations at all levels above. It is computed by extrapolating the wavefield perturbation from the level above $\Delta\mathcal{U}_z$, plus the scattered wavefield at this level $\Delta\mathcal{V}_{z+\Delta z}$.

Equation (5) is also a recursive equation which can be written in matrix form as

$$\begin{pmatrix} 1 & 0 & 0 & \cdots & 0 & 0 \\ -\mathbf{E}_0 & 1 & 0 & \cdots & 0 & 0 \\ 0 & -\mathbf{E}_1 & 1 & \cdots & 0 & 0 \\ \vdots & \vdots & \vdots & \ddots & \vdots & \vdots \\ 0 & 0 & 0 & \cdots & -\mathbf{E}_{n-1} & 1 \end{pmatrix} \begin{pmatrix} \Delta\mathcal{U}_0 \\ \Delta\mathcal{U}_1 \\ \Delta\mathcal{U}_2 \\ \vdots \\ \Delta\mathcal{U}_n \end{pmatrix} \\ = \begin{pmatrix} 0 & 0 & 0 & \cdots & 0 & 0 \\ \Delta\mathbf{E}_0 & 0 & 0 & \cdots & 0 & 0 \\ 0 & \Delta\mathbf{E}_1 & 0 & \cdots & 0 & 0 \\ \vdots & \vdots & \vdots & \ddots & \vdots & \vdots \\ 0 & 0 & 0 & \cdots & \Delta\mathbf{E}_{n-1} & 0 \end{pmatrix} \begin{pmatrix} \mathcal{U}_0 \\ \mathcal{U}_1 \\ \mathcal{U}_2 \\ \vdots \\ \mathcal{U}_n \end{pmatrix}$$

or in a more compact notation as

$$(\mathbf{1} - \mathbf{E})\Delta\mathcal{U} = \Delta\mathbf{E}\mathcal{U}. \quad (6)$$

The operator $\Delta\mathbf{E}$ represents a perturbation of the extrapolation operator \mathbf{E} . The quantity $\Delta\mathbf{E}\mathcal{U}$ represents a scattered wavefield, and is a function of the perturbation in the medium given by the scattering relationships derived in Appendix A. For the case of single scattering, we can write

$$\Delta\mathcal{V}_{z+\Delta z} \equiv \Delta\mathbf{E}_z[\mathcal{U}_z] = \mathbf{E}_z[\mathbf{S}_z(\tilde{\mathcal{U}}_z)[\Delta s_z]]. \quad (7)$$

The expression for the total wavefield perturbation $\Delta\mathcal{U}$ obtained from (5) becomes

$$\Delta\mathcal{U}_{z+\Delta z} = \mathbf{E}_z[\Delta\mathcal{U}_z] + \mathbf{E}_z[\mathbf{S}_z(\tilde{\mathcal{U}}_z)[\Delta s_z]], \quad (8)$$

which is also a recursive relationship that can be written in matrix form as

$$\begin{pmatrix} 1 & 0 & 0 & \cdots & 0 & 0 \\ -\mathbf{E}_0 & 1 & 0 & \cdots & 0 & 0 \\ 0 & -\mathbf{E}_1 & 1 & \cdots & 0 & 0 \\ \vdots & \vdots & \vdots & \ddots & \vdots & \vdots \\ 0 & 0 & 0 & \cdots & -\mathbf{E}_{n-1} & 1 \end{pmatrix} \begin{pmatrix} \Delta\mathcal{U}_0 \\ \Delta\mathcal{U}_1 \\ \Delta\mathcal{U}_2 \\ \vdots \\ \Delta\mathcal{U}_n \end{pmatrix} \\ = \begin{pmatrix} 0 & 0 & 0 & \cdots & 0 & 0 \\ \mathbf{E}_0 & 0 & 0 & \cdots & 0 & 0 \\ 0 & \mathbf{E}_1 & 0 & \cdots & 0 & 0 \\ \vdots & \vdots & \vdots & \ddots & \vdots & \vdots \\ 0 & 0 & 0 & \cdots & \mathbf{E}_{n-1} & 0 \end{pmatrix} \begin{pmatrix} \mathcal{U}_0 \\ \mathcal{U}_1 \\ \mathcal{U}_2 \\ \vdots \\ \mathcal{U}_n \end{pmatrix} \\ + \begin{pmatrix} \mathbf{S}_0 & 0 & 0 & \cdots & 0 \\ 0 & \mathbf{S}_1 & 0 & \cdots & 0 \\ 0 & 0 & \mathbf{S}_2 & \cdots & 0 \\ \vdots & \vdots & \vdots & \ddots & \vdots \\ 0 & 0 & 0 & \cdots & \mathbf{S}_n \end{pmatrix} \begin{pmatrix} \Delta s_0 \\ \Delta s_1 \\ \Delta s_2 \\ \vdots \\ \Delta s_n \end{pmatrix}$$

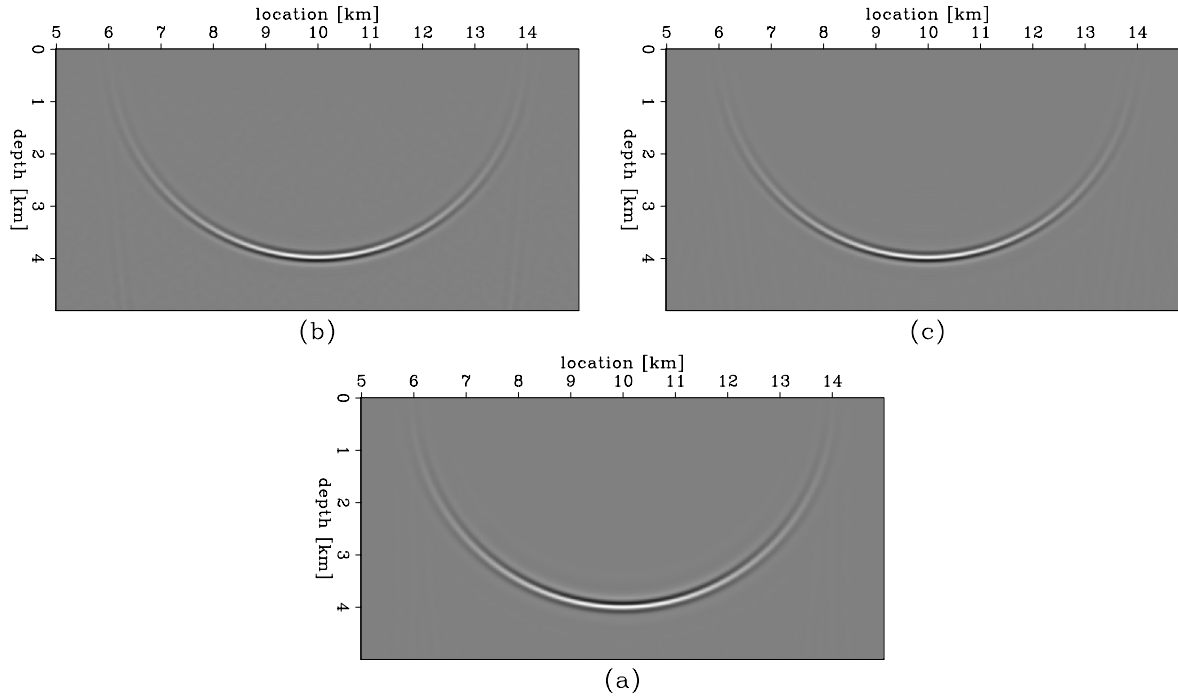


Figure 1 Comparison of image perturbations obtained as the difference between two migrated images (b) and as the result of the forward WEMVA operator applied to the known slowness perturbation (c). (a) shows the background image corresponding to the background slowness. Since the slowness perturbation is small (0.1%), the image perturbations in (b) and (c) are practically identical.

or in a more compact notation as

$$(1 - E) \Delta \mathcal{U} = E S \Delta s. \quad (9)$$

The vector Δs denotes the slowness perturbation at all depths.

Finally, if we introduce the notation,

$$\mathbf{G} = (1 - E)^{-1} E S, \quad (10)$$

we can write a simple relationship between a slowness perturbation Δs and the corresponding wavefield perturbation $\Delta \mathcal{U}$:

$$\Delta \mathcal{U} = \mathbf{G} \Delta s. \quad (11)$$

This expression describes wavefield scattering caused by the interaction of the background wavefield with a perturbation of the medium.

MIGRATION VELOCITY ANALYSIS

Migration velocity analysis is based on estimating the velocity that optimizes certain properties of the migrated images. In general, measuring such properties involves making a transformation after wavefield extrapolation to the migrated image,

using a function f , so that

$$\mathcal{P}_z = f \mathbf{I}_z [\mathcal{U}_z], \quad (12)$$

where \mathbf{I} is the imaging operator applied to the extrapolated wavefield \mathcal{U} . In compact matrix form, we can write this relationship as

$$\mathcal{P} = f(\mathbf{I}\mathcal{U}). \quad (13)$$

The image \mathcal{P} is subject to optimization from which we derive the velocity updates.

Two examples of transformation functions are:

- $f(x) = x - t$ where t is a known target. A WEMVA method based on this criterion optimizes

$$\mathcal{P}_z = \mathbf{I}_z [\mathcal{U}_z] - \mathbf{I}_z [\mathcal{T}_z], \quad (14)$$

where \mathcal{T}_z denotes the target wavefield. This is called a *target image fitting* (TIF) method (Biondi and Sava 1999; Sava and Fomel 2002).

- $f(x) = D x$ where D is a known operator. A WEMVA method based on this criterion optimizes

$$\mathcal{P}_z = \mathbf{D}_z [\mathbf{I}_z [\mathcal{U}_z]]. \quad (15)$$

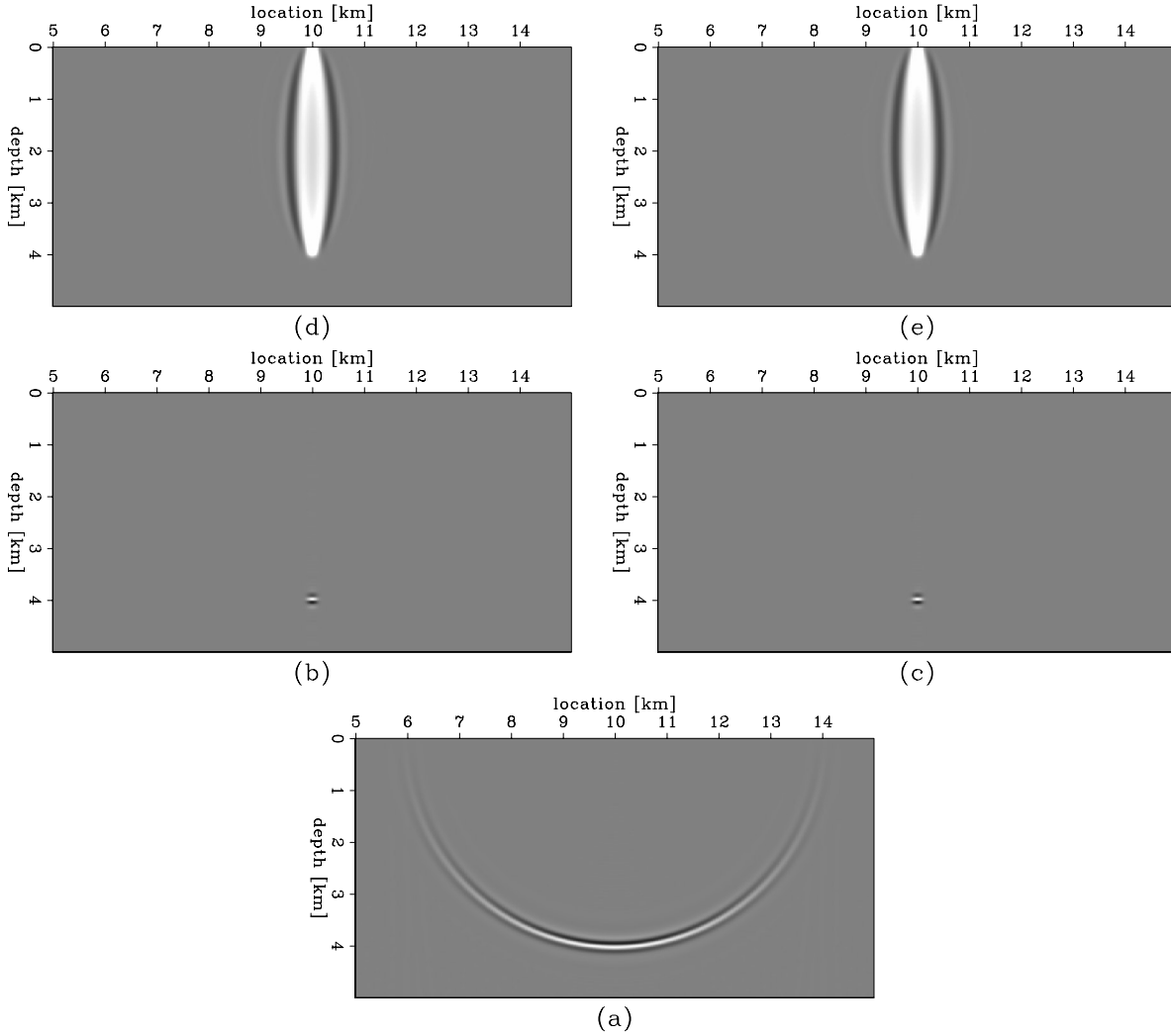


Figure 2 Comparison of slowness backprojections using the WEMVA operator applied to image perturbations computed as the difference between two migrated images, (b) and (d), and as the result of the forward WEMVA operator applied to a known slowness perturbation, (c) and (e). (a) shows the background image corresponding to the background slowness. Since the slowness perturbation is small (0.1%), the image perturbations in (b) and (c) and the fat rays in (d) and (e) are practically identical.

If \mathbf{D} is a differential semblance operator, this is called a *differential semblance optimization* (DSO) method (Symes and Carazzone 1991; Shen 2003).

In general, such transformations belong to a family of affine functions that can be written as

$$\mathcal{P}_z = \mathbf{A}_z[\mathcal{I}_z[\mathcal{U}_z]] - \mathbf{B}_z[\mathcal{I}_z[\mathcal{T}_z]], \tag{16}$$

or in compact matrix form as

$$\mathcal{P} = \mathbf{A}\mathcal{U} - \mathbf{B}\mathcal{T}, \tag{17}$$

where the operators \mathbf{A} and \mathbf{B} are known and take special forms depending on the optimization criterion used. For example,

$\mathbf{A} = \mathbf{1}$ and $\mathbf{B} = \mathbf{1}$ for TIF, and $\mathbf{A} = \mathbf{D}$ and $\mathbf{B} = \mathbf{0}$ for DSO. $\mathbf{1}$ denotes the identity operator and $\mathbf{0}$ denotes the null operator. With the definition in (16), we can write the objective function J as

$$J(s) = \frac{1}{2} \sum_{z,m,h} |\mathcal{P}_z|^2 \tag{18}$$

$$= \frac{1}{2} \sum_{z,m,h} |\mathbf{A}_z[\mathcal{I}_z[\mathcal{U}_z]] - \mathbf{B}_z[\mathcal{I}_z[\mathcal{T}_z]]|^2, \tag{19}$$

where s is the slowness function, and z , \mathbf{m} , \mathbf{h} denote, respectively, depth and the midpoint and offset vectors. In compact

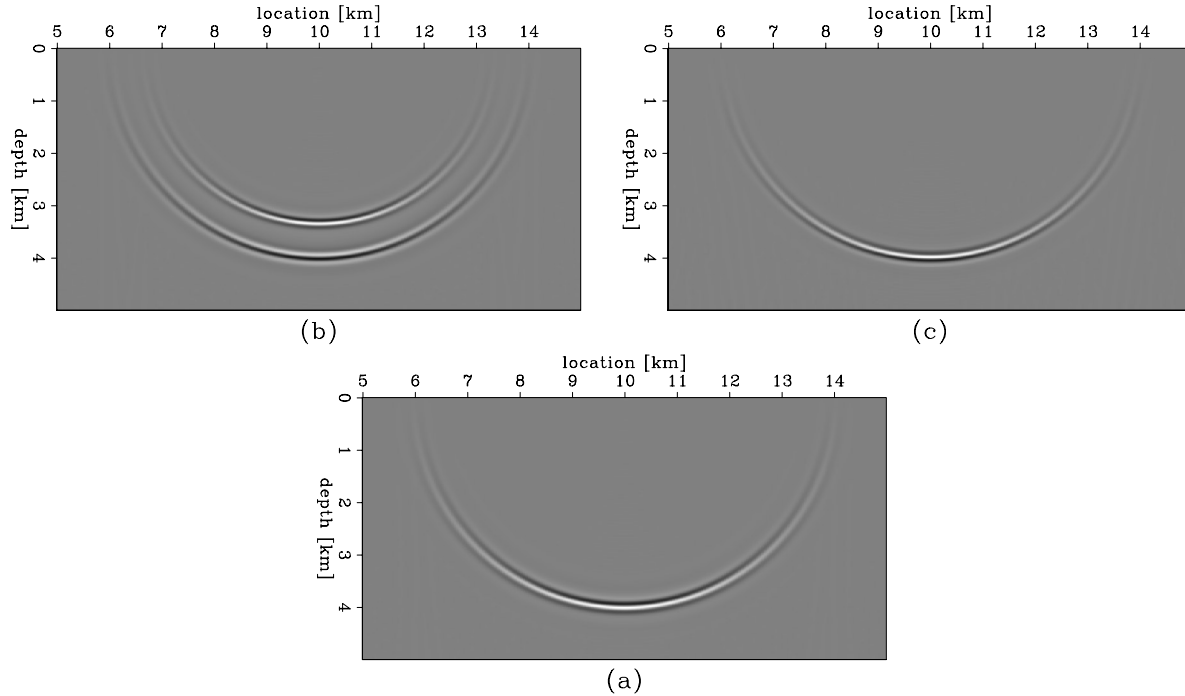


Figure 3 Comparison of image perturbations obtained as the difference between two migrated images (b) and as the result of the forward WEMVA operator applied to the known slowness perturbation (c). (a) shows the background image corresponding to the background slowness. Since the slowness perturbation is large (20%), the image perturbations in (b) and (c) are different from one another.

matrix form, we can write the objective function as

$$J(s) = \frac{1}{2} |\mathbf{A}\mathbf{U} - \mathbf{B}\mathbf{I}\mathbf{T}|^2. \quad (20)$$

In the Born approximation, the total wavefield \mathbf{U} is related to the background wavefield $\tilde{\mathbf{U}}$ by the linear relationship,

$$\mathbf{U} \approx \tilde{\mathbf{U}} + \mathbf{G}\Delta s. \quad (21)$$

If we can replace the total wavefield in the objective function (20), we obtain

$$J(s) = \frac{1}{2} |\mathbf{A}\tilde{\mathbf{U}} - \mathbf{B}\mathbf{I}\mathbf{T} + \mathbf{A}\mathbf{G}\Delta s|^2. \quad (22)$$

Equation (22) describes a linear optimization problem, in which we obtain Δs by minimizing the objective function,

$$J(\Delta s) = |\Delta\mathcal{R} - \mathbf{L}\Delta s|^2, \quad (23)$$

where $\Delta\mathcal{R} = -(\mathbf{A}\tilde{\mathbf{U}} - \mathbf{B}\mathbf{I}\mathbf{T})$ and $\mathbf{L} = \mathbf{A}\mathbf{G}$. The operator \mathbf{L} is constructed, based on the Born approximation (Lo and Inderweisen 1994), and involves the pre-computed background wavefield through the background medium. The implementation details for operator \mathbf{L} are discussed in Appendix

A. The convex optimization problem defined by the linearization in (22) can be solved using standard conjugate-gradient techniques.

Since, in most practical cases, the inversion problem is not well conditioned, we need to add constraints on the slowness model via a regularization operator. In these situations, we use the modified objective function,

$$J(\Delta s) = |\Delta\mathcal{R} - \mathbf{L}\Delta s|^2 + \epsilon^2 |\mathbf{A}\Delta s|^2. \quad (24)$$

Here, \mathbf{A} is a regularization operator, and ϵ is a scalar parameter that balances the relative importance of the data residual $(\Delta\mathcal{R} - \mathbf{L}\Delta s)$ and the model residual $(\mathbf{A}\Delta s)$.

We illustrate our method with a simple model, shown in Fig. 1. The velocity is constant and the data are represented by an impulse in space and time. We consider two slowness models: one regarded as the correct slowness s_c and the other as the background slowness \tilde{s} . The two slownesses are related by a scaling factor $\rho = s_c/\tilde{s}$. For this example, we take $\rho = 1.001$ to ensure that we do not violate the requirements imposed by the Born approximation.

Next, we migrate the data with the background slowness \tilde{s} and store the extrapolated wavefield at all depth

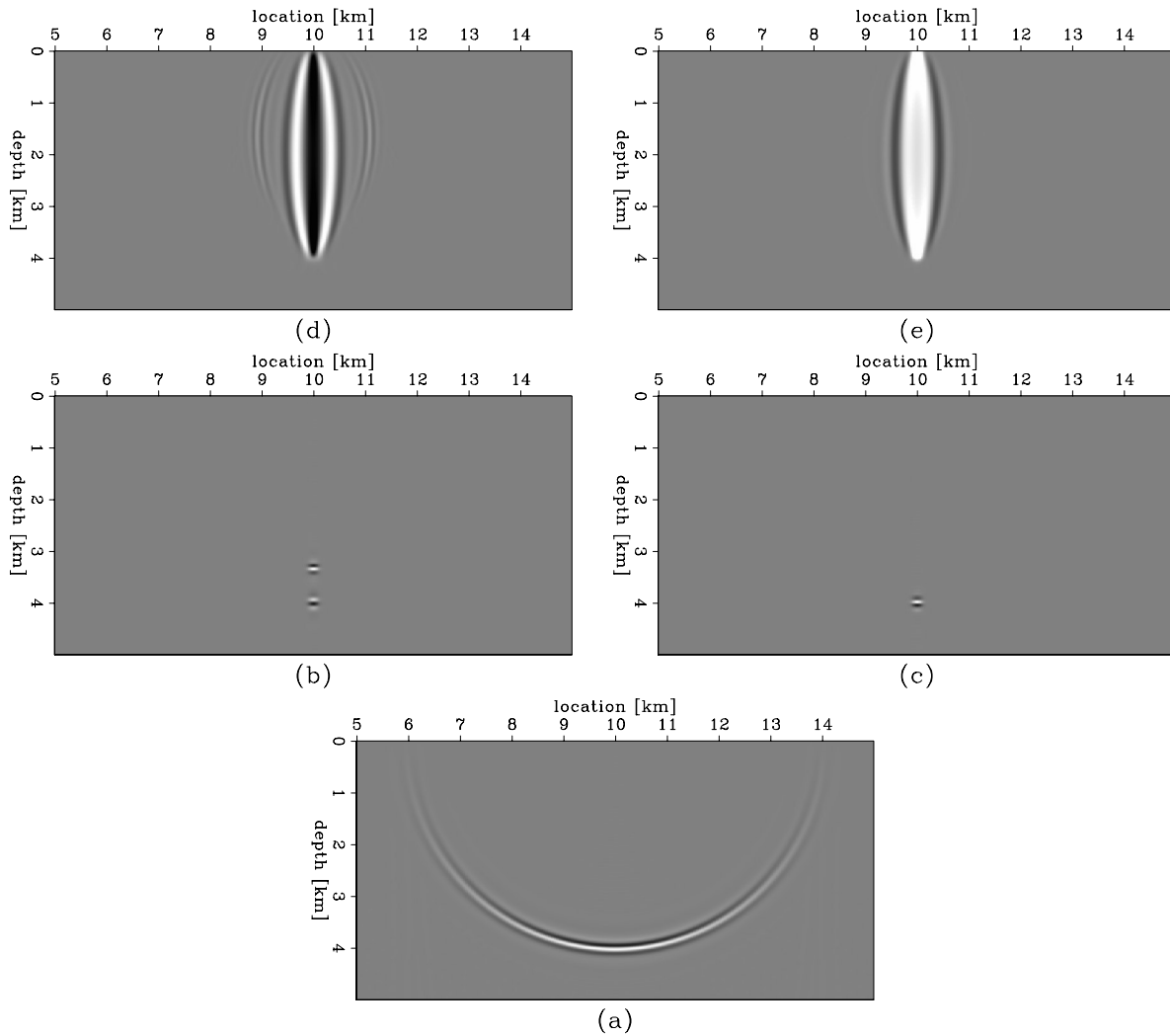


Figure 4 Comparison of slowness backprojections using the WEMVA operator applied to image perturbations computed as the difference between two migrated images, (b) and (d), and as the result of the forward WEMVA operator applied to a known slowness perturbation, (c) and (e). (a) shows the background image corresponding to the background slowness. Since the slowness perturbation is large (20%), the image perturbations in panels (b) and (c) and the fat rays in (d) and (e) are different from one another. (d) shows the typical behaviour associated with the breakdown of the Born approximation.

levels. Figure 1(a) shows the image corresponding to the background slowness $\tilde{\mathcal{R}}$. We also migrate the data with the correct slowness and obtain a second image \mathcal{R}_c . A simple subtraction of the two images gives the image perturbation in Fig. 1(b).

Finally, we compute an image perturbation by a simple application of the forward WEMVA operator, defined in (23), to the slowness perturbation $\Delta s = s_c - \tilde{s}$ (Fig. 1c). Since the slowness perturbation is very small, the requirements imposed by the Born approximation are fulfilled, and the two images in Figs 1(b) and 1(c) are identical. The image perturbations are phase-shifted by 90° relative to the background image.

A simple illustration of the adjoint operator L , defined in (23), is shown in Fig. 2. Figure 2(a) shows the background image, Figs 2(b) and 2(c) show image perturbations, and Figs 2(d) and 2(e) show slowness perturbations. We extract a small subset of each image perturbation to create the impulsive image perturbations shown in Figs 2(b) and 2(c). Figures 2(b) and 2(d) correspond to the image perturbation computed as an image difference, while Figs 2(c) and 2(e) correspond to the image perturbation computed with the forward WEMVA operator. In this way, our data correspond to a single point on the surface, and our image perturbation corresponds to a single point in the subsurface. By backprojecting the image

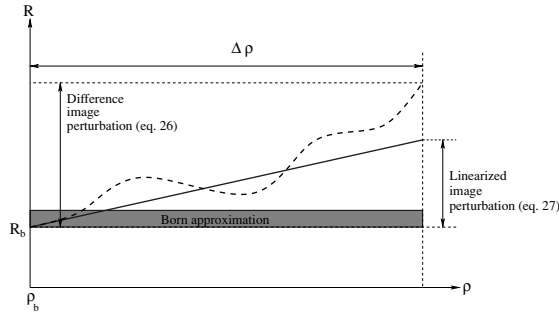


Figure 5 A schematic description of our method for computing linearized image perturbations, showing images on the vertical axis and function of velocity on the horizontal axis. The dashed line corresponds to image changes described by residual migration with various values of the velocity ratio parameter ρ . The straight solid line corresponds to the linearized image perturbation computed with an image gradient operator applied to the reference image, scaled at every point by the difference of the velocity ratio parameter $\Delta\rho$.

perturbations in Figs 2(b) and 2(c) with the adjoint WEMVA operator, we obtain identical ‘fat rays’ shown in Figs 2(d) and 2(e), respectively.

IMAGE PERTURBATION BY RESIDUAL MIGRATION

Prestack Stolt residual migration (PSRM) can be used to create image perturbations (Sava 2003). Given an image migrated with the background velocity, we can construct another image by using an operator \mathbf{K} , a function of the parameter ρ that represents the ratio of the original and modified velocities. The improved velocity map is not known explicitly, although it is described indirectly by the ratio map of the two velocities:

$$\mathcal{R} = \mathbf{K}(\rho) [\tilde{\mathcal{R}}]. \quad (25)$$

The simplest form of an image perturbation can be constructed as a difference between an *improved* image \mathcal{R} and the *background* image $\tilde{\mathcal{R}}$, given by

$$\Delta\mathcal{R} = \mathcal{R} - \tilde{\mathcal{R}}. \quad (26)$$

The main challenge with this method of constructing image perturbations for WEMVA is that the two images can be phase-shifted too much with respect to one another. Thus, we violate the requirements of the Born approximation and risk subtracting images that are out of phase. This problem is common in all wavefield-based velocity analysis or tomographic methods using the Born approximation (Woodward 1992; Pratt 1999; Dahlen *et al.* 2000).

A simple illustration of the problem is shown in Figs 3 and 4. This example is similar to the one shown in Figs 1 and 2, except that the velocity ratio linking the two slownesses is much larger, i.e. $\rho = 1.20$. In this case, the background and correct images are out of phase, and when we subtract them we obtain two distinct events, as shown in Fig. 3(b). In contrast, the image perturbation obtained by the forward WEMVA operator (Fig. 3c) shows only one event, as in the previous example. The only difference between the image perturbations in Figs 1(c) and 3(c) is a scaling factor related to the magnitude of the slowness anomaly.

Figure 4 shows fat rays for each kind of image perturbation: Figs 4(b) and 4(d) show the image perturbations obtained by subtraction of the two images, and Figs 4(c) and 4(e) show the image perturbation obtained by applying the forward WEMVA operator. The fat rays corresponding to the ideal image perturbation (Figs 4c and 4e) do not change from the previous example, except for the scaling factor. However, in the case when we use image differences (Figs 4b and 4d), we violate the requirements of the Born approximation. In this case, we see slowness backprojections of opposite sign relative to the true anomaly, and we also see two characteristic migration ellipsoidal side-events, indicating cycle skipping (Woodward 1992).

We address this problem by employing linearized image perturbations. If we define $\Delta\rho = \rho - 1$, we can write a discrete version of the image perturbation, using a Taylor series expansion of (25), as

$$\Delta\mathcal{R} \approx \mathbf{K}'|_{\rho=1} [\tilde{\mathcal{R}}] \Delta\rho, \quad (27)$$

where the ‘ \prime ’ sign denotes derivation relative to the velocity ratio parameter ρ . Image perturbations computed with (27) are known as *linearized image perturbations*. Figure 5 illustrates this procedure.

The linearized PSRM operator $\mathbf{K}'|_{\rho=1}$ can be computed analytically, as described in Appendix B. With this operator, we can compute linearized image perturbations in two steps. First, we run residual migration for a large range of velocity ratios and at every image point we pick the ratio which maximizes the flatness of the gathers. We then apply the operator in (27) to the background image $\tilde{\mathcal{R}}$ and scale the result with the picked $\Delta\rho$.

The linearized image perturbations approximate the non-linear image perturbations caused by arbitrary velocity model changes. They are based on the gradient of the image change relative to a velocity model change, and are less restrictive than the Born approximation limits.

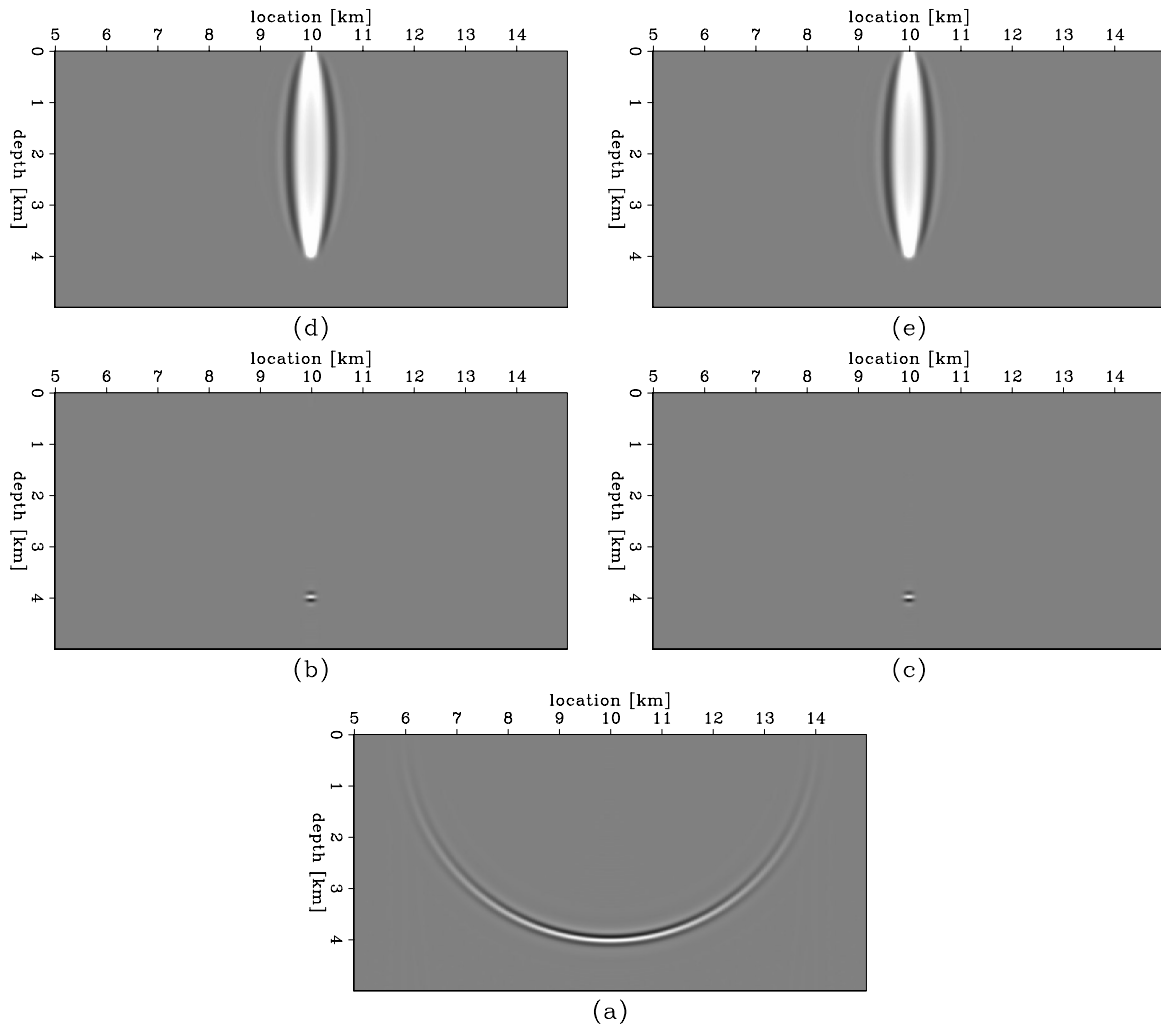


Figure 6 Comparison of slowness backprojections using the WEMVA operator applied to image perturbations computed with the differential image perturbation operator, (b) and (d), and as the result of the forward WEMVA operator applied to a known slowness perturbation, (c) and (e). (a) shows the background image corresponding to the background slowness. Despite the fact that the slowness perturbation is large (20%), the image perturbations in (b) and (c) and the fat rays in (d) and (e) are practically identical, both in shape and in magnitude.

Figure 6 shows how the linearized image perturbation methodology applies to the synthetic example used above. All panels are similar to those in Figs 2 and 4, except that Figs 6(b) and 6(d) correspond to linearized image perturbations, instead of simple image perturbations. Again, we compare image and slowness perturbations with the ideal perturbations obtained by the forward WEMVA operator (Figs 6c and 6e). Both the image and slowness perturbations are identical in shape and magnitude.

Inversion example

Our next example concerns linearized image perturbations computed for prestack images. We use another simple model

with flat reflectors and constant velocity. The image perturbation methodology is identical to the one outlined in the preceding paragraphs. The main point of this example is to illustrate our methodology in a situation where the requirements of the first-order Born approximation are clearly violated. In this case, the slowness perturbation is 50% of the background slowness.

Figure 7 shows representative common-image gathers in the angle domain (Sava and Fomel 2003) for (a) the background image, (b) the correct image, (c) the image perturbation obtained as a difference of the two images, (d) the image perturbation obtained using the forward WEMVA operator, and (e) the linearized image perturbation. Figures 7(d) and 7(e)

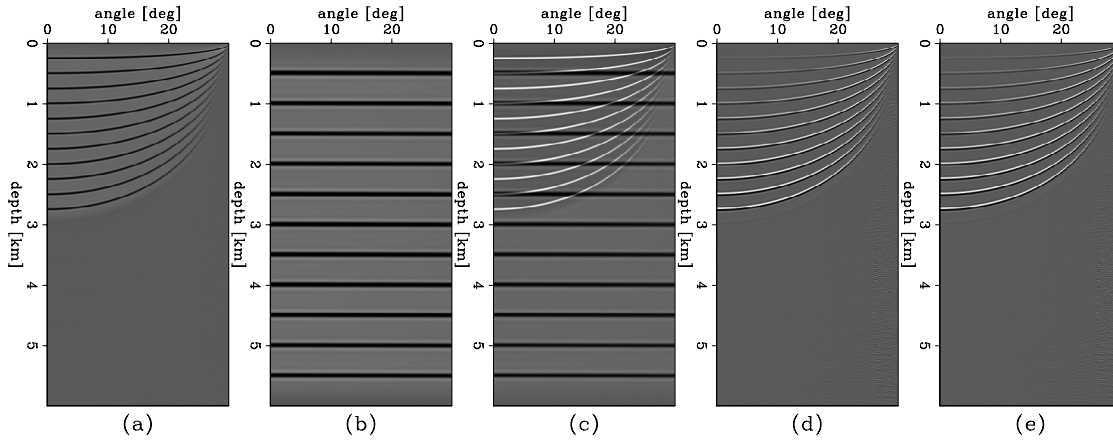


Figure 7 Comparison of common-image gathers for image perturbations obtained as the difference between two migrated images (c), as the result of the forward WEMVA operator applied to the known slowness perturbation (d), and as the result of the differential image perturbation operator applied to the background image (e). (a) shows the background image corresponding to the background slowness, and (b) shows an improved image obtained from the background image using residual migration. Despite the fact that the slowness perturbation is large (50%), the image perturbations in (b) and (c) are identical within numerical accuracy.

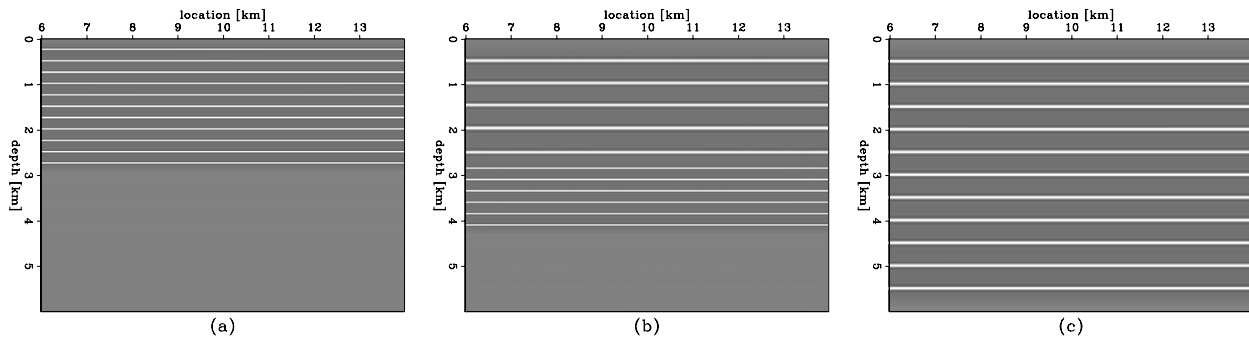


Figure 8 WEMVA applied to a simple model with flat reflectors. (a) The background image; (b) the image updated after one non-linear iteration; (c) the image computed with the correct slowness.

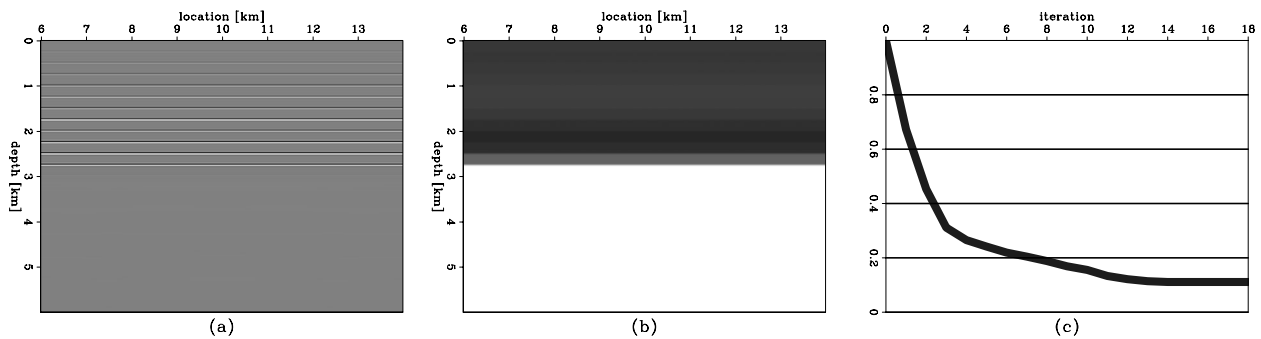


Figure 9 WEMVA applied to a simple model with flat reflectors. (a) The zero-offset of the image perturbation; (b) the slowness update after the first non-linear iteration; (c) the convergence curve of the first linear iteration.

are identical within numerical accuracy, indicating that our methodology can be successfully employed to create correct image perturbations well beyond the limits of the first-order Born approximation.

Finally, we apply our migration velocity analysis algorithm to the example in Fig. 7. First, we compute the background wavefield represented by the background image (Figs 7a and 8a). Next, we compute the linearized image perturbation, shown in Fig. 9(a) (stack) and in Fig. 7(e) (angle gather from the middle of the image).

From this image perturbation, we invert for the slowness perturbation (Fig. 9b). We stop the inversion after 19 linear iterations when the data residual has stopped decreasing (Fig. 9c). The slowness updates occur in the upper half of the model. Since no reflectors exist in the bottom part of the model, no slowness update is computed for this region.

Finally, we remigrate the data using the updated slowness and obtain the image in Fig. 8(b). For comparison, Fig. 8(c) shows the image obtained after migration with the correct slowness. The two images are identical in the upper half where we have updated the slowness model. Further updates to the model would require more non-linear iterations.

CONCLUSIONS

We present a new migration velocity analysis method using wavefield extrapolation techniques that can address the challenges posed by velocity estimation in complicated media with sharp contrasts and fine-scale features. Our method is formulated in the migrated image space, with an objective function aimed at improving the image quality. The method is based on a linearization of the downward-continuation operator that relates perturbations of slowness models to perturbations of migrated images. Since our method is based on finite-difference extrapolation of band-limited waves, it naturally takes into account the multipathing that characterizes wave propagation in complex environments with large and sharp velocity contrasts. It also takes into account the full wavefield information, and not only selectively picked traveltimes, as is currently the case in state-of-the-art traveltome tomography.

We use prestack Stolt residual migration to define image perturbations by maximizing the focusing and the flatness of angle-domain common-image gathers. In general, the image perturbations computed with this method can be too different from the background image, and we are in danger of subtracting images that are not in phase, violating our first-order Born approximation assumption. We avoid divergence of the

inversion procedure when the velocity perturbations are too large, by not inverting directly the image perturbations obtained by residual migration, but by inverting linearized versions of them. Thus, we achieve a method which is robust with respect to large model perturbations, a crucial step for a practical MVA method.

We illustrate our method with simple numerical examples, and show that our method is well behaved even for large slowness perturbations, well beyond the limits of the first-order Born approximation. A companion paper (Sava and Biondi 2004) illustrates the full potential of our method with more complex examples.

ACKNOWLEDGEMENT

We acknowledge the financial support of the sponsors of Stanford Exploration Project.

REFERENCES

- Biondi B. 1997. Azimuth moveout + common-azimuth migration: Cost-effective prestack depth imaging of marine data. 67th SEG meeting, Dallas, USA, Expanded Abstracts, 1375–1378.
- Biondi B. and Palacharla G. 1996. 3D prestack migration of common-azimuth data. *Geophysics* 61, 1822–1832.
- Biondi B. and Sava P. 1999. Wave-equation migration velocity analysis. 69th SEG meeting, Houston, USA, Expanded Abstracts, 1723–1726.
- Bunks C., Saleck F.M., Zaleski S. and Chavent G. 1995. Multiscale seismic waveform inversion. *Geophysics* 60, 1457–1473.
- Chavent G. and Jacewitz C.A. 1995. Determination of background velocities by multiple migration fitting. *Geophysics* 60, 476–490.
- Claerbout J.F. 1985. *Imaging the Earth's Interior*. Blackwell Scientific Publications.
- Dahlen F.A., Hung S.H. and Nolet G. 2000. Fréchet kernels for finite frequency traveltimes—I. Theory. *Geophysical Journal International* 141, 157–174.
- Forgues E., Scala E. and Pratt R.G. 1998. High-resolution velocity model estimation from refraction and reflection data. 68th SEG meeting, New Orleans, USA, Expanded Abstracts, 1211–1214.
- de Hoop M., le Rousseau J.H. and Wu R.S. 1996. Generalization of the phase-screen approximation for the scattering of acoustic waves. *Wave Motion* 31, 43–70.
- Huang L.Y., Fehler M.C. and Wu R.S. 1999. Extended local Born Fourier migration method. *Geophysics* 65, 1524–1534.
- Hung S.H., Dahlen F.A. and Nolet G. 2000. Fréchet kernels for finite frequency traveltimes—II. Examples. *Geophysical Journal International* 141, 175–203.
- Lo T.W. and Inderweisen P.L. 1994. *Fundamentals of Seismic Tomography*. Society of Exploration Geophysicists.
- Mosher C.C., Foster D.J. and Hassanzadeh S. 1997. Common angle imaging with offset plane waves. 67th SEG meeting, Dallas, USA, Expanded Abstracts, 1379–1382.

- Noble M., Lindgren J. and Tarantola A. 1991. Large-sized nonlinear inversion of a marine data set: Retrieving the source, the background velocity and the impedance contrasts. 61st SEG meeting, Houston, USA, Expanded Abstracts, 893–896.
- O'Brien M.J. and Etgen J.T. 1998. Wavefield imaging of complex structures with sparse, point-receiver data. 68th SEG meeting, New Orleans, USA, Expanded Abstracts, 1365–1368.
- Popovici A.M. 1996. Prestack migration by split-step DSR. *Geophysics* **61**, 1412–1416.
- Pratt A.M. 1999. Seismic waveform inversion in the frequency domain, Part I: Theory and verification in a physical scale model. *Geophysics* **64**, 888–901.
- Ristow D. and Rühl T. 1994. Fourier finite-difference migration. *Geophysics* **59**, 1882–1893.
- Sava P. 2003. Prestack residual migration in the frequency domain. *Geophysics* **67**, 634–640.
- Sava P. and Biondi B. 2004. Wave-equation migration velocity analysis. II. Examples. *Geophysical Prospecting* **52**, 607–623.
- Sava P. and Fomel S. 2002. Wave-equation migration velocity analysis beyond the Born approximation. 72nd SEG meeting, Salt Lake City, USA, Expanded Abstracts, 2285–2288.
- Sava P. and Fomel S. 2003. Angle-domain common image gathers by wavefield continuation methods. *Geophysics* **68**, 1065–1074.
- Shen P. 2003. Differential semblance velocity analysis by wave-equation migration. 73rd SEG meeting, Dallas, USA, Expanded Abstracts, 2132–2135.
- Symes W.W. and Carazzone J.J. 1991. Velocity inversion by differential semblance optimization. *Geophysics* **56**, 654–663.
- Woodward M.J. 1992. Wave-equation tomography. *Geophysics* **57**, 15–26.
- Yilmaz O. 1979. *Prestack partial migration*. PhD thesis, Stanford University.

APPENDIX A

The scattering operator

Imaging by wavefield extrapolation (WE) is based on recursive continuation of wavefields \mathcal{U} from a given depth level to the next by means of an extrapolation operator \mathbf{E} . Within every extrapolation slab, we can write

$$\mathcal{U}_{z+\Delta z} = \mathbf{E}_z [\mathcal{U}_z], \quad (\text{A1})$$

where \mathcal{U}_z is the wavefield at the top of the slab, and $\mathcal{U}_{z+\Delta z}$ is the wavefield at the bottom of the slab. The operator \mathbf{E} involves a spatially dependent phase shift described by

$$\mathbf{E}_z[\cdot] = e^{ik_z \Delta z}, \quad (\text{A2})$$

where k_z is the depth wavenumber and Δz is the wavefield extrapolation depth step. (A1) corresponds to the analytical solution of the differential equation,

$$\mathcal{U}'(z) = ik_z \mathcal{U}(z), \quad (\text{A3})$$

which describes depth extrapolation of monochromatic plane waves (Claerbout 1985). The ' sign represents a derivative with respect to the depth z . The depth wavenumber k_z is given by the one-way wave equation, also known as the single square root equation,

$$k_z = \sqrt{\omega^2 s^2 - |\mathbf{k}|^2}, \quad (\text{A4})$$

where ω is the temporal frequency, s is the laterally variable slowness of the medium and \mathbf{k} is the horizontal wavenumber. We use s and \mathbf{k} in (A4) for conciseness, although such a notation is not mathematically correct in laterally varying media.

Since downward continuation by Fourier-domain phase shift can be applied for slowness models that vary only with depth, we need to split the operator \mathbf{E} into two parts: a constant slowness *continuation operator* applied in the $(\omega - \mathbf{k})$ domain, which accounts for the propagation in depth, and a *screen operator* applied in the $(\omega - \mathbf{x})$ domain, which accounts for the wavefield perturbations due to the lateral slowness variations. In essence, we approximate the vertical wavenumber k_z with its constant slowness counterpart k_{z0} , corrected by a term describing the spatial variability of the slowness function (Ristow and Rühl 1994).

Furthermore, we can separate the depth wavenumber k_z into two components, one corresponding to the background medium \tilde{k}_z and one corresponding to a perturbation of the medium:

$$k_z = \tilde{k}_z + \Delta k_z. \quad (\text{A5})$$

In a first-order approximation, we can relate these two depth wavenumbers by a Taylor series expansion:

$$k_z \approx \tilde{k}_z + \left. \frac{dk_z}{ds} \right|_{s=\tilde{s}} (s - \tilde{s}) \quad (\text{A6})$$

$$\approx \tilde{k}_z + \omega \frac{\omega \tilde{s}}{\sqrt{\omega^2 \tilde{s}^2 - |\mathbf{k}|^2}} (s - \tilde{s}), \quad (\text{A7})$$

where $s(z, \mathbf{x})$ is the slowness corresponding to the perturbed medium and $\tilde{s}(z)$ is the background slowness.

Within any depth slab, we can extrapolate the wavefield from the top, either in the perturbed or in the background medium. The wavefields at the bottom of the slab, $\tilde{\mathcal{U}}_{z+\Delta z} = \mathcal{U}_z e^{i\tilde{k}_z \Delta z}$ and $\mathcal{U}_{z+\Delta z} = \mathcal{U}_z e^{ik_z \Delta z}$, are related by the relationship:

$$\mathcal{U}_{z+\Delta z} \approx \tilde{\mathcal{U}}_{z+\Delta z} e^{i\Delta k_z \Delta z}. \quad (\text{A8})$$

Equation (A8) is a direct statement of the Rytov approximation (Lo and Inderweisen 1994), since the wavefields at the bottom of the slab correspond to different phase shifts related by a linear equation.

The wavefield perturbation $\Delta\mathcal{V}$ at the bottom of the slab is obtained by subtracting the background wavefield $\tilde{\mathcal{U}}$ from the perturbed wavefield \mathcal{U} :

$$\Delta\mathcal{V}_{z+\Delta z} \approx \mathcal{U}_{z+\Delta z} - \tilde{\mathcal{U}}_{z+\Delta z} \quad (\text{A9})$$

$$\approx (e^{i\Delta k_z \Delta z} - 1) \tilde{\mathcal{U}}_{z+\Delta z} \quad (\text{A10})$$

$$\approx e^{i\tilde{k}_z \Delta z} \left(e^{i \frac{dk_z}{ds} \Big|_{s=\tilde{s}} \Delta s_z \Delta z} - 1 \right) \tilde{\mathcal{U}}_z, \quad (\text{A11})$$

where $\Delta s = s - \tilde{s}$ is the perturbation between the correct and the background slownesses at depth z .

In operator form, we can write

$$\Delta\mathcal{V}_{z+\Delta z} = \mathbf{E}_z [\mathbf{R}_z (\tilde{\mathcal{U}}_z) [\Delta s_z]], \quad (\text{A12})$$

where \mathbf{E}_z represents the downward-continuation operator at depth z , and \mathbf{R}_z represents the *Rytov* scattering operator, which is dependent on the background wavefield $\tilde{\mathcal{U}}_z$ and the slowness perturbation Δs_z at that depth level, and is given by

$$\mathbf{R}_z (\tilde{\mathcal{U}}_z) [\Delta s_z] = \left(e^{i \frac{dk_z}{ds} \Big|_{s=\tilde{s}} \Delta s_z \Delta z} - 1 \right) \tilde{\mathcal{U}}_z. \quad (\text{A13})$$

In this approximation, we assume that the scattered wavefield is generated only by the background wavefield and we ignore all multiscattering effects. For the Born approximation (Lo and Inderweisen 1994), we further assume that the wavefield differences are small, so that we can linearize the exponential according to the relationship $e^{i\Delta\phi} \approx 1 + i\Delta\phi$. With this new approximation, the expression for the downward-continued scattered wavefield becomes

$$\Delta\mathcal{V}_{z+\Delta z} \approx e^{i\tilde{k}_z \Delta z} \left(i \frac{dk_z}{ds} \Big|_{s=\tilde{s}} \Delta s_z \Delta z \right) \tilde{\mathcal{U}}_z. \quad (\text{A14})$$

In operator form, we can write the scattered wavefield at z as

$$\Delta\mathcal{V}_{z+\Delta z} = \mathbf{E}_z [\mathbf{S}_z (\tilde{\mathcal{U}}_z) [\Delta s_z]], \quad (\text{A15})$$

where \mathbf{E}_z represents the downward-continuation operator at depth z , and \mathbf{S}_z represents the *Born* scattering operator, which is dependent on the background wavefield and operates on the slowness perturbation at that depth level.

The linear scattering operator \mathbf{S} is a mixed-domain operator similar to the extrapolation operator \mathbf{E} . This operator is related to the background wavefield and background slowness by the expression:

$$\mathbf{S}_z (\tilde{\mathcal{U}}_z) [\Delta s_z] \approx i \frac{dk_z}{ds} \Big|_{s=\tilde{s}} \Delta z \Delta s_z \tilde{\mathcal{U}}_z. \quad (\text{A16})$$

In practice, we can implement the scattering operator described by (A16) in different ways:

- One option is to implement the Born operator (A16) in the space domain using an expansion (Huang, Fehler and Wu 1999) such as

$$\frac{dk_z}{ds} \Big|_{s=\tilde{s}} \approx \omega \left(1 + \frac{1}{2} \left[\frac{|\mathbf{k}|}{\omega \tilde{s}} \right]^2 + \frac{3}{8} \left[\frac{|\mathbf{k}|}{\omega \tilde{s}} \right]^4 + \frac{5}{16} \left[\frac{|\mathbf{k}|}{\omega \tilde{s}} \right]^6 + \frac{35}{128} \left[\frac{|\mathbf{k}|}{\omega \tilde{s}} \right]^8 + \dots \right). \quad (\text{A17})$$

In practice, the summation of the terms in (A17) involves forward and inverse fast Fourier transforms (FFT and IFT) and multiplication in the space domain with the spatially variable \tilde{s} , i.e.

$$\Delta\mathcal{V}_z = i\omega\Delta z\Delta s_z \left[1 + \sum_{j=1,\dots} c_j \frac{1}{(\omega\tilde{s})^{2j}} \text{IFT}[|\mathbf{k}|^{2j} \text{FFT}[\tilde{\mathcal{U}}_z]] \right], \quad (\text{A18})$$

where $c_j = \frac{1}{2}, \frac{3}{8}, \dots$.

- Another option is to implement the Born operator (A16) in the Fourier domain relative to the constant reference slowness in any individual slab. In this case, we can write

$$\frac{dk_z}{ds} \Big|_{s=s_0} \approx \omega \frac{\omega s_0}{\sqrt{\omega^2 s_0^2 - (1 - i\eta)^2 |\mathbf{k}|^2}}, \quad (\text{A19})$$

where η is a damping parameter which avoids division by zero (de Hoop, le Rousseau and Wu 1996). In practice, the implementation of (A19) involves FFT and IFT, i.e.

$$\Delta\mathcal{V}_z = i\Delta z \text{IFT} \left[\frac{dk_z}{ds} \Big|_{s=s_0} \text{FFT}[\tilde{\mathcal{U}}_z \Delta s_z] \right]. \quad (\text{A20})$$

APPENDIX B

Linearized image perturbations

A linearized image perturbation is computed using a residual migration operator \mathbf{K} in a relationship such as

$$\Delta\mathcal{R} \approx \mathbf{K}'|_{\rho=1} [\tilde{\mathcal{R}}] \Delta\rho. \quad (\text{B1})$$

The operator \mathbf{K} depends on the scalar parameter ρ which is the ratio of the velocity to which we residually migrate and the background velocity. The background image corresponds to $\rho = 1$.

Using the chain rule of differentiation, we can write

$$\Delta\mathcal{R} \approx \frac{d\mathbf{K}}{dk_z} \frac{dk_z}{d\rho} \Big|_{\rho=1} [\tilde{\mathcal{R}}] \Delta\rho, \quad (\text{B2})$$

where k_z is the depth wavenumber defined for PSRM.

Equation (B2) offers the possibility of building the image perturbation directly, by computing three elements: the derivative of the image with respect to the depth wavenumber and two weighting functions, one for the derivative of the depth wavenumber with respect to the velocity ratio parameter (ρ), and the other one for the magnitude of the $\Delta\rho$ perturbation from the reference to the improved image.

Firstly, the image derivative in the Fourier domain, $\frac{dK}{dk_z}$, is straightforward to compute in the space domain as

$$\left. \frac{dK}{dk_z} \right|_{\rho=1} [\tilde{\mathcal{R}}] = -iz\tilde{\mathcal{R}}. \quad (\text{B3})$$

The derivative image is simply the imaginary part of the migrated image, scaled by depth.

Secondly, we can obtain the weighting representing the derivative of the depth wavenumber with respect to the velocity ratio parameter, $\left. \frac{dk_z}{d\rho} \right|_{\rho=1}$, starting from the double square

root equation written for prestack Stolt residual migration (Sava 2003):

$$\begin{aligned} k_z &= k_{zs} + k_{zr} \\ &= \frac{1}{2}\sqrt{\rho^2\mu^2 - |\mathbf{k}_s|^2} + \frac{1}{2}\sqrt{\rho^2\mu^2 - |\mathbf{k}_r|^2}, \end{aligned}$$

where μ is given by the expression,

$$\mu^2 = \frac{[4(k_{zo})^2 + (\mathbf{k}_r - \mathbf{k}_s)^2][4(k_{zo})^2 + (\mathbf{k}_r + \mathbf{k}_s)^2]}{16k_{zo}^2}. \quad (\text{B4})$$

The derivative of k_z with respect to ρ is

$$\frac{dk_z}{d\rho} = \rho \left(\frac{\mu^2}{4k_{zs}} + \frac{\mu^2}{4k_{zr}} \right), \quad (\text{B5})$$

therefore

$$\left. \frac{dk_z}{d\rho} \right|_{\rho=1} = \frac{\mu^2}{2\sqrt{\mu^2 - |\mathbf{k}_s|^2}} + \frac{\mu^2}{2\sqrt{\mu^2 - |\mathbf{k}_r|^2}}. \quad (\text{B6})$$